Thermal Characterization of Single Event Burnout Failure in Semiconductor Power Devices

D. G. Walker and T. S. Fisher
Department of Mechanical Engineering
Vanderbilt University
Box 1592, Station B
Nashville, TN 37235
greg.walker@vanderbilt.edu
tim.fisher@vanderbilt.edu

J. Liu and R. D. Schrimpf
Department of Electrical Engineering
Vanderbilt University
Box 1824, Station B
Nashville, TN 37235
liuj1@vuse.vanderbilt.edu
ron.schrimpf@vanderbilt.edu

Abstract

Previous experimental investigations of single event burnout of power devices due to heavy ion impacts have been performed to identify the conditions required to result in failure of devices. To verify these findings, simulations have been performed that model the burnout with limited success. Although simulations provide order-of-magnitude estimates as well as prediction of phenomenological features, they have not provided completely quantitative agreement to measurements and cannot characterize all experimental data. By describing the temperature response to the burnout event using an analytic conduction solution, secondary electrical features can be characterized. Further, it is believed that simulation modeling can be advanced through the inclusion of temperature models. This work, therefore, represents a first attempt to characterize thermal failure of power devices due to heavy ion impacts. The thermal model in the present work produces qualitative agreement with experiments on single-event burnout that have been previously unexplained.

Nomenclature

α	thermal diffusivity
E_g	band gap energy (J)
g	volumetric generation rate (W/m^3)
k	thermal conductivity (W/m^2 K)
k_b	Boltzmann constant (1.38e-23 J/K)
N	effective density of states (cm^{-3})
n_i	intrinsic carrier concentration (cm^{-3})
q	electron/hole charge (C)
r	radius (μm)
T	temperature (K)
μ	carrier mobility (cm^2/volt-sec)

I. Introduction

Single-event burnout (SEB) failure of power devices may result from heavy ion impacts that occur in space environments [1, 2]. The failure of electronic components in structures such as satellites and high-altitude aircraft that operate in ion rich environments can be detrimental to the survival of the vehicles. Research in the area of SEB of power devices can, therefore, reduce the incidence of catastrophic failures of power devices and thereby increase the survivability of aerospace structures. The ability to model SEB events can augment the design process leading to more reliable devices and equipment that depend on these devices.

SEB is triggered when a heavy ion passes through a power MOSFET biased in the "off" state (blocking a high drain-source voltage). As a high energy ion travels through the device, a path of electron-hole pairs are created [3]. As a result, a "current-filament" along the path of the ion is induced. This initial short-lived induced current then causes the MOSFET to "turn on". Once the MOSFET has been activated in this way, the device may remain on due to the parasitic bipolar-junction transistor (BJT) inherent in the device [4].

The source, body, and drain regions of the MOSFET comprise the emitter, base, and collector regions of the parasitic BJT respectively. The BJT in the model is the mechanism by which the MOSFET is activated by the ion strike. During normal operation of the power MOSFET, this parasitic BJT is always turned off due to the common source-body metallization that shorts the base-emitter junction. Transient currents generated by heavy ion impacts turn on the parasitic BJT of the power MOSFET by inducing a current between the source and

0-7803-5916-X/00/$10.00 ©2000 IEEE

drain. Due to a regenerative feedback mechanism, collector currents in the BJT increase to the point where secondary breakdown can occur, creating a permanent short between the source and drain, rendering the MOSFET useless [5].

Numerous studies have been conducted to investigate the SEB mechanism and its effects on power MOSFETs [6]. Models developed to explain the SEB phenomenon have been very helpful in gaining insight into the physical failure mechanisms that contribute to SEB. An SEB circuit model has been developed for understanding the SEB dependence on the various circuit parameters [7].

Modeling and simulation of SEB remain as important methods of determining why heavy ion impact results in destructive currents and provide a means for performing virtual experiments that are less expensive than physical tests. However, modeling has not been able to describe induced currents and burnout accurately even though trends and order-of-magnitude analyses agree at times. This disparity between electrical simulation models and experimental data is due primarily to the incomplete description of energy transport mechanisms. Consequently, the power dissipation in the form of thermal energy has often been ignored in the analysis. It is accepted that the failure mechanism is ultimately a result of thermal melt-down, but the effect of the energy generated on the electrical properties and behavior has not been previously considered in detail.

Prior work on SEB phenomena includes experimental investigations of several types of power devices, including MOSFETs [8] and IGBTs [9]. These tests measured the electrical response to heavy ion impacts. For appropriate conditions, the devices were errantly turned on by the induced current of the ion impact. The resulting current is frequently self-maintaining and must be cut off to avoid destruction of the device. Because of experimental limitations, an incomplete set of parameters that are influential in determining the possibility of failure have been identified and bounded.

Representative measurements of Joule heating as a result of self-maintaining currents from heavy ion collisions range from 5W [8] to nearly 100W [9]. Furthermore, the generation of this power is concentrated in a small region [6] and lasts for several micro-seconds (until the device is turned off to prevent melt-down). These values are indicative of non-equilibrium effects as shown by Apanovich et al. [10] whose work indicates that simulation must incorporate nonisothermal effects to eliminate inaccuracies for devices with small features and large temperature gradients. Although the present work does not include non-equilibrium effects between energy carrying particles, it does represent a characterization of the influence of temperature on relevant transport mechanisms.

The objective of this work is to characterize the generation of thermal energy in SEB of power devices using an analytic conduction solution coupled with a circuit-level electrical simulation. From the temperature fields obtained in this analysis, electrical effects such as carrier concentration and mobility, which are highly coupled to the thermal response, are inferred. Also, the thermal simulations are coupled to SPICE to demonstrate the effects of increased temperature on device performance. Lastly, the assumptions concerning the generation region will be investigated through parametric studies of temperature as a function of the geometry of the region of heat generation.

Because of the low fidelity of the models used in this investigation, quantitative results are limited. This analysis does not replace a comprehensive electro-thermal simulation with non-equilibrium energy transport. However, we can extract valuable information about the effects of temperature during SEB events and predict to some degree the behavior of devices.

II. Theory and Model Development

A. Electrical Model

The SEB process can be modeled as an electrical circuit shown in Figure 1 [7]. Several key elements are used to model the SEB process. A linear current pulse represents the initial current at the junction. A resistor connects the body region to the source, which corresponds to the base resistance in the SEB analytical model [6]. When a heavy ion hits the device, the deposited charges will charge the RC circuit and raise the base voltage. Depending on how high the initial base voltage is increased, the parasitic BJT may be turned on. A feedback mechanism is then established which is modeled by a current-controlled current source in the circuit model. The thermal effect on the device is represented by a variable shunt resistance R_{TC} parallel with the parasitic BJT.

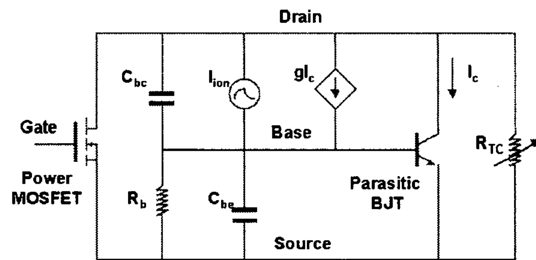

Figure 1: Electrical circuit used to model SEB of power MOSFETs.

The only components in the SPICE model that are temperature dependent are the parasitic BJT and the shunt resistance. The temperature dependence of the transistor is controlled by SPICE's model parameters and is a weak function of temperature. Therefore, the model

without the shunt resistance produces negligible effects as the temperature is changed. The shunt resistance, then, is the single most important component when incorporating temperature effects, and is solely responsible for the results reported here. The evaluation of this resistance is described in a subsequent section.

B. Analytic Conduction Model

The transient, non-homogeneous diffusion equation is solved analytically for boundary conditions and properties representative of an operating power device undergoing a heavy ion strike (see Figure 2 for computational domain). To find a solution, we assume that the heat generation occurs in a cylindrical region surrounding the current filament, and the governing equation is solved in an axisymmetric cylindrical coordinate system.

$$\frac{1}{r}\frac{\partial}{\partial r}\left(r\frac{\partial T}{\partial r}\right)+\frac{\partial^2 T}{\partial z^2}+\frac{g}{k}=\frac{1}{\alpha}\frac{\partial T}{\partial t} \tag{1}$$

Here, g is a constant generation rate per unit volume, and the thermal conductivity (k) and thermal diffusivity (α) are assumed to be independent of temperature. The boundary conditions for the disk-shaped conduction domain (depicted in Figure 3) are insulated at the centerline (because of symmetry) and insulated in the far-field. The top of the device is insulated and the bottom is held at a constant temperature.

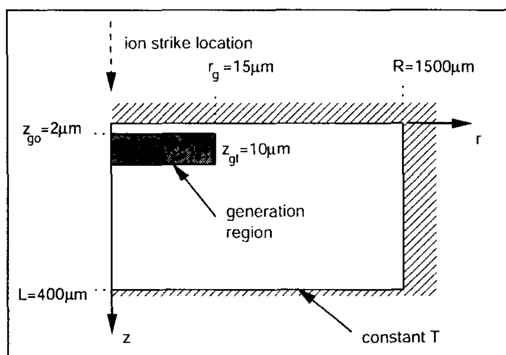

Figure 2: The computational domain is cylindrical where the current filament lies along the centerline.

The geometry of the conduction problem is correlated to the geometry of the device shown in Figure 3. The insulated boundaries lie on the top and bottom surface of the device and the centerline ($r = 0$) runs vertically through the middle of the gate where the electron flow is greatest. The Joule heating occurs about the centerline in the n-region (epitaxial) where the electron flow is greatest during the burnout event. Because of the time scales used in this analysis, it can be assumed that the conduction domain in the axial and radial directions are semi-infinite. Therefore, it is worth mentioning that the generation region is close to the top surface of the chip because the substrate in Figure 3 is roughly 400 μm, which is much larger than the dimensions used for the generation region.

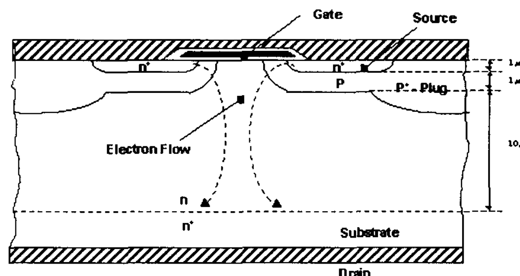

Figure 3: The dimensions of a typical MOSFET device were used as guidelines for determining the computational domain of the conduction analysis.

The generation region is specified by a radius of influence r_g, the longitudinal location (z_{go}) and a thickness (z_{gl}). Therefore, the values for the location and thickness were taken to be $z_{go} = 2\,\mu$m and $z_{gl} = 10\,\mu$m respectively. The radius of the generation region was a free parameter in the problem and could take a value from the radius of the current filament to the size of a single cell of the MOSFET. The power (P), dissipated in this region due to Joule heating, is estimated from circuit voltages and currents. Since the intensity of the generation is determined by the volume (or area for two dimensional analysis) of the region in which generation occurs, the effects of size and location can significantly influence the results.

The conduction solution results in a temperature field from which a representative temperature must be chosen. This representative temperature is passed to the electrical analysis as the operating temperature of the circuit. Within the generation region, the temperature distribution is relatively flat so the maximum temperature is used to model the temperature effects in the circuit analysis. Therefore, all components that depend on temperature will be affected. Additionally, the temperature was used to calculate the shunt resistance from an intrinsic carrier concentration (see section C).

The solution of Equation 1 involves integral transforms and produces an infinite series [11]. The computation of the series was verified for convergence and accuracy by testing against other known one dimensional solutions. Furthermore, the transient solution was seen to approach the independent two dimensional steady state solution. Additionally the number of terms used in the two dimensional transient analysis was increased by an order of magnitude to ensure convergence (as we are not especially concerned with computational time here).

C. Shunt Resistance Model

The shunt resistance included in the SPICE circuit is the primary coupling between the thermal analysis and

the electrical circuit model. Even though temperature dependence is built into the BJT in the circuit, its dependence is relatively weak compared to the effects of the shunt resistor.

Since the resistor represents the electrical resistance through the epitaxial layer of the power MOSFET, its magnitude is largely governed by the intrinsic carrier concentration (n_i) in the device (see reference [12]).

$$R_{\mathrm{TC}} = \frac{1}{q\mu n_i}\frac{l}{A} \tag{2}$$

Here, q is the charge of the carriers, μ is the mobility of the carriers, l is the length of the epitaxial region or the distance through which the current is resisted, and A is the area of the resistor. Note that the mobility is considered constant in this case because its functionality on temperature is fairly weak and highly dependent on the level of doping.

At normal operating temperatures, R_{TC} is very large and does not play a significant role in the circuit. As the temperature increases, the shunt resistance decreases until it eventually dominates the electrical conduction. The intrinsic carrier concentration and the area of resistance are both functions of temperature that cause the resistance to decrease with temperature.

The resistance area is circular region defined by the radius of the generation region plus a distance defined by the penetration depth of the thermal energy. It is assumed that the penetration depth can be expressed as in terms of the thermal diffusivity and time ($r_p = \sqrt{\alpha t}$). The energy generated from Joule heating diffuses into the surrounding area raising the temperature outside the generation region thus increasing the effective area of the shunt resistance.

The intrinsic carrier concentration is used in the modeling of the shunt resistor because at high temperatures it will become larger than the doping. The temperature-dependent carrier concentration [12] which is a strong function of temperature is given as

$$n_i = \sqrt{N_C N_V}\exp\left[-\frac{E_g}{2k_b T}\right] \tag{3}$$

where the band gap ($E_g = 10^{-19}\,\mathrm{J}$), and the effective density of states for the conduction band (N_C) and the valence band (N_V) are evaluated for silicon. The effective density of states for silicon can be written as [13].

$$N_C = 2.8\mathrm{e}19\left(\frac{T}{300}\right)^{3/2} \tag{4}$$

$$N_V = 1.04\mathrm{e}19\left(\frac{T}{300}\right)^{3/2} \tag{5}$$

Initially temperature is not a factor in controlling the shunt resistance. At normal operating temperatures, the dopant concentration overwhelms the intrinsic concentration. This initial concentration is accounted for in the model of the MOSFET in SPICE and is therefore not considered in the shunt resistance. Once the concentration due to a rise in temperature exceeds the dopant concentration, the shunt resistance becomes significant in the overall model.

III. Results

A. Conduction Solution

The temperature of most interest is the maximum temperature, which strongly affects electrical behavior. The power dissipated was estimated from experimental data and circuit level analysis to be approximately 8W. Figure 4 shows the maximum temperature for this power level. After 0.5 μsec, the temperature rise has reached 300 K. Assuming the operating temperature of a device is around 350 K, the maximum temperature approaches the melting temperature of aluminum. Even though the melting temperature of aluminum may not be a deciding factor in the survivability of a device, it demonstrates the potential for catastrophic failure. Clearly, temperature is a significant factor in the electric behavior of the device long before melt-down actually occurs.

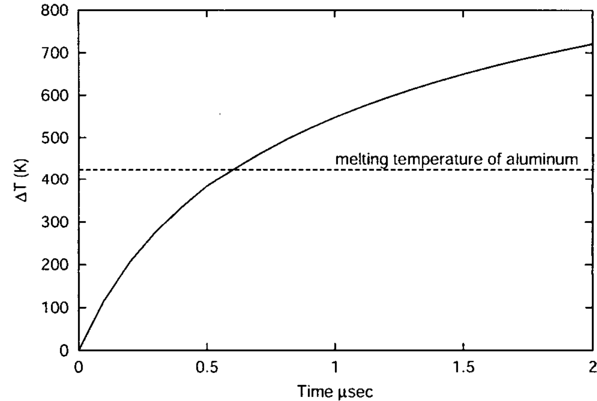

Figure 4: The maximum temperature reaches metallic melting temperature in a little over .5 μsec.

Note that the location of the maximum temperature is initially in the center of the generation region on the centerline. With increasing time, the boundary conditions (namely the insulated top surface of the chip) begin to influence the solution more. As a result, the location of maximum temperature moves towards the top of the device. Figure 5 displays the distribution of temperature at the centerline of the device for different times.

The localization of temperature can be seen from Figure 6, which illustrates the temperature rise near the generation site at 0.5 μsec. Even though the central temperatures are very high, the energy has not diffused far from the generation site, and large gradients ensue.

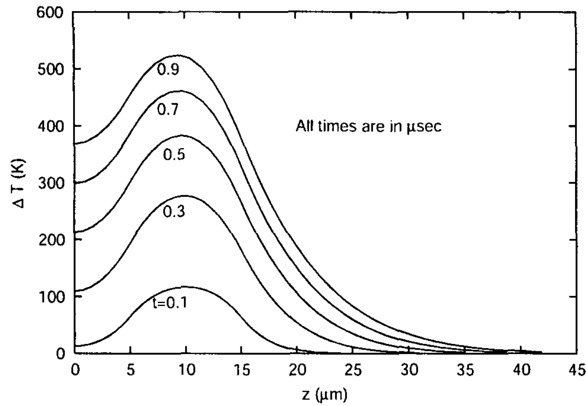

Figure 5: The temperature distribution along the location of the current filament represents the maximum temperature at any given time.

For this reason, the maximum temperature, can provide a good estimate of the representative temperature of the circuit. At $t = 0.5\,\mu$sec, the heat flux can be estimated using Fourier's Law to be $10^9\,\mathrm{W/m^2}$, which is roughly two orders of magnitude greater than the flux on the surface of the Sun.

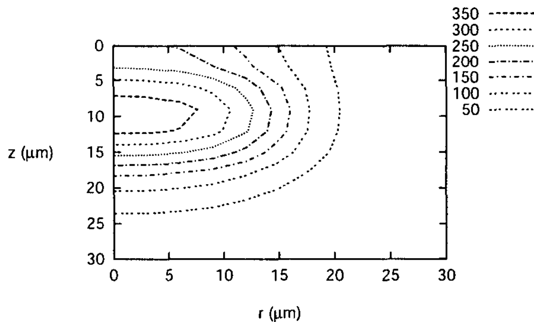

Figure 6: Temperature contours at $t = 0.5\mu$sec indicate the localization of the heat generation.

B. Circuit-level results

Without including the temperature as a feedback parameter in the circuit analysis, we can obtain an estimate of the power dissipated in a power device as a result of an ion strike. From Figure 7, we notice that the device is "turned on" by the ion strike at $t = 1\,\mu$sec. The device then remains on for the duration of the simulation without any significant change in the calculations. For the circuit parameters selected [7] and without incorporating the temperature rise, there is no evidence of a secondary rise in the current. Note that without the shunt resistor, an increase in temperature does not significantly affect the results shown despite the fact that the BJT is temperature dependent.

Using the current and voltage time histories, the power dissipated can be estimated to be approximately 8W. Recall that Figure 4 represents the temperature rise due to 8W being dissipated in a single cell of the power MOSFET device. Therefore, we can expect a similar temperature rise for this particular device.

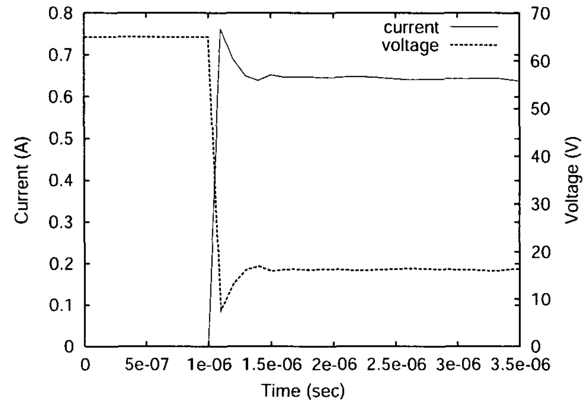

Figure 7: Typical voltage and current response due to a heavy ion strike at $t = 1\,\mu$sec calculated from a circuit level analysis without thermal effects.

C. Coupled Electrical/Thermal Results

As stated earlier, the primary goal of this work is to introduce thermal analysis into the circuit level electrical analysis in an attempt to describe a phenomenon reported by Roubaud et al. [8] in MOSFETs and again by Lorfèvre et al. [9] in IGBTs. Given appropriate conditions, power devices have been known to exhibit a secondary increase in current between $0.3\,\mu$sec and $0.6\,\mu$sec after the ion strike. Representative data are given in Figure 8(a) and 8(b). It is believed that the secondary increase in current is caused by a large increase in temperature. We have seen that the Joule heating resulting from the ion strike, can cause a device to reach temperatures near survivability limits of some of the components.

The coupling of the temperature solution and SPICE was accomplished by first wrapping the SPICE model and the conduction analysis. The SPICE wrapper then started and stopped SPICE's transient analysis at small time increments. For each time step, a temperature using the conduction solution and Duhamel's theorem for an arbitrarily varying generation rate was obtained. The resulting maximum temperature was then used as the component temperature in the SPICE model. Between each step the current "state" of the electrical analysis was recorded so it could be reset to start the analysis for the subsequent time step. This integration approach is similar to that used by Van Petegem, et al. [14].

The result of the coupled analysis is a secondary peak

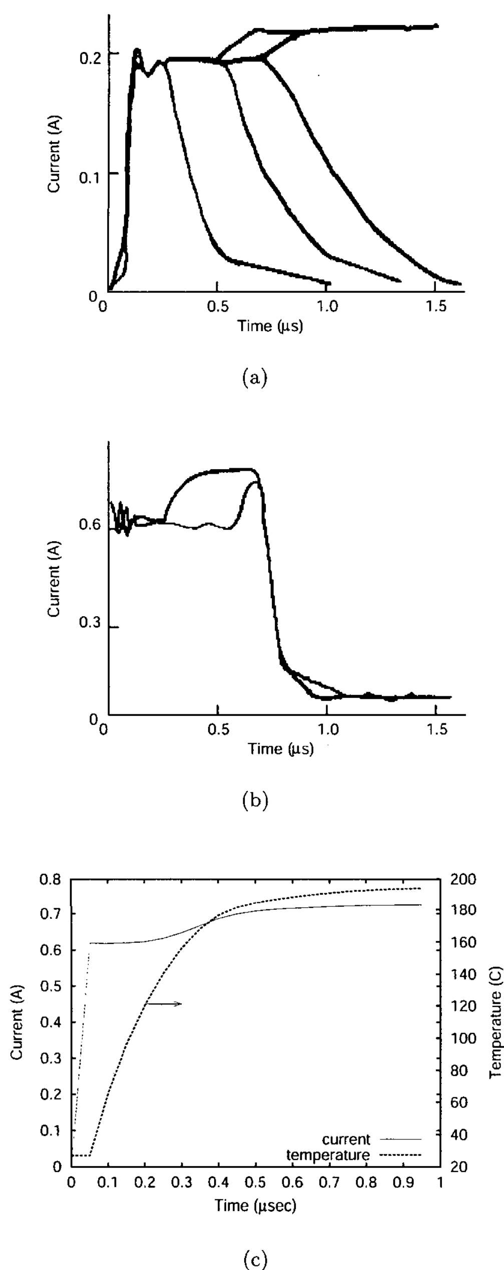

Figure 8: Representative experimental data reported by (a) Johnson et al. [5] and (b) Roubaud, et al. [8] along with (c) simulated current response and temperature history.

in the current that resembles the experimental data (see Figure 8(c)). The predicted secondary rise is not as steep as the experimental data. Furthermore, the time when the rise occurs is slightly earlier than in the experiment.

What is not shown in Figure 8(c), is that the temperature reaches a maximum. Notice that the rate of the temperature rise decreases significantly once the device reaches its new operating point. At the higher current, the voltage is actually smaller which results in a smaller amount of power being dissipated. It turns out, that the amount of power matches the rate at which the energy is diffused resulting in a relatively constant temperature. This suggests that if the temperature where that the device ultimately settles is lower than any destructive temperature, catastrophic failure will not be reached.

Several analytical approximations affect the ability of the coupled model to match the experimental data more precisely. The more influential factors include the characteristic temperature used to represent the temperature of the entire device. The analytic conduction solution is capable of generating a temperature field, but we must select a single temperature for the circuit analysis. Similarly, the generation region shape and size will affect the results. In our case, we assumed a cylinder which extended over the epitaxial region using the radius as a free parameter. In reality the generation is not confined to and is not constant through the defined region. Despite these approximations along with other standard assumptions such as constant thermal properties, the present model predicts the occurrence of the secondary current rise. More detailed modeling should improve the model's ability to predict the event's onset time, rise time and magnitude.

As mentioned previously, devices that experience temperature increases in such short time periods are often thrown out of thermodynamic equilibrium. A device is considered to be out of equilibrium when the local energy carriers in the device have significantly different energy levels. This effect was not considered in this simplified model. Additional research that includes electro-thermal modeling of statistical device physics is needed to resolve non-equilibrium effects.

D. Generation Region

Using the data acquired in section C as a baseline, the effect of the size and shape of the generation region on the secondary rise in current can be investigated. The free parameter in this case is the radius of the generation region. As the radius decreases, we expect the temperature to increase since the same amount of power is being dissipated in a smaller region. If we take the radius of the generation region to be on the order of the current filament, unreasonable temperatures are calculated. Therefore, the region must be larger than the radius of the filament. The range of values for the radius that produce reasonable results is shown in Figure 9. The metrics that identify the character of the peak are the start time, the rise time and the increase in current. As expected, a larger radius smoothes the peak out and delays its onset because the temperature does not rise as rapidly.

For comparison, the metrics for the representative experimental data shown in Figure 8(a) and 8(b) and the baseline simulated analysis are given in Table 1

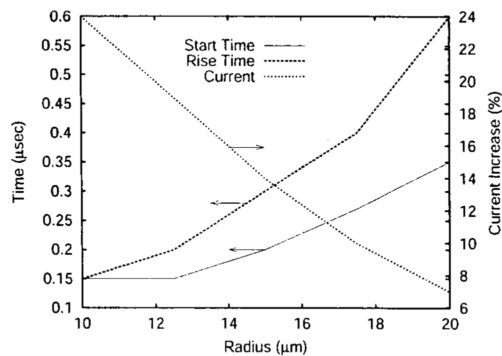

Figure 9: Secondary peak metrics as a function of generation region radius.

Table 1
Secondary peak metrics for data displayed in Figure 8. Times are in micro-seconds.

Metric	Exp (a)	Exp (b)	Sim (c)
Start Time	0.5	0.3	0.2
	0.75	0.65	
Rise Time	0.2	0.1	0.3
	0.2	0.15	
Current Rise	16%	25%	14%
	16%	24%	

IV. Conclusions

It was shown that in the case of single event burnout of power devices, simulations cannot neglect the immense temperature rise resulting from power dissipation from an ion strike event. From an analytic conduction solution using voltage-current measurements as an estimate of the thermal energy diffusing into a device, the temperature resulting from a heavy ion strike was characterized for the first time. The coupled electrical thermal solution demonstrated qualitative agreement with experimental data.

V. Acknowledgements

Thanks go to Scott Humphreys, Masters Student in Electrical Engineering at Vanderbilt University for his expertise in using SPICE and getting it to do things it was not designed to do. This work was supported by a Discovery Grant from Vanderbilt University.

VI. References

[1] A. E. Waskiewicz, J. W. Groninger, V. H. Strahan, and D. M. Long, "Burnout of power mos transistors with heavy ions of 252-Cf," *IEEE Transactions on Nuclear Science*, vol. 33, pp. 1710–1713, 1986.

[2] P. T. Ma and P. V. Dressendorfer, *Ionizing Radiation Effects in MOS Devices and Circuits.* New York: Wiley, 1989.

[3] J. H. Hohl and G. H. Johnson, "Features of the triggering mechanism for single event burnout of power MOSFETs," *IEEE Transactions on Nuclear Science*, vol. 36, pp. 2260–2266, Dec. 1989.

[4] J. H. Hohl and K. F. Galloway, "Analytical model for single event burnout of power MOSFETs," *IEEE Transactions on Nuclear Science*, vol. 34, pp. 1275–1280, Dec. 1987.

[5] G. H. Johnson, J. Palau, C. Dachs, K. F. Galloway, and R. D. Schrimpf, "A review of the techniques used for modeling single-event effects in power mosfets," *IEEE Transactions on Nuclear Science*, vol. 43, pp. 546–560, 1996.

[6] G. H. Johnson, J. H. Hohl, R. D. Schrimpf, and K. F. Galloway, "Simulating single-event burnout of n-channel power MOSFET's," *IEEE Transactions on Electron Devices*, vol. 40, pp. 1001–1008, May 1993.

[7] J. Liu, "Modeling of single event burnout in n-channel power mosfets," Master's thesis, Vanderbilt University, Jan. 2000.

[8] F. Roubaud, C. Dachs, J.-M. Palau, J. Gasiot, and P. Tastet, "Experimental and 2D simulation study of the single-event burnout in n-channel power MOSFET's," *IEEE Transactions on Nuclear Science*, vol. 40, pp. 1952–1958, Dec. 1993.

[9] E. Lorfèvre, C. Dachs, C. Detcheverry, J.-M. Palau, J. Gasiot, F. Roubaud, M.-C. Calvert, and R. Ecoffet, "Heavy ion induced failures in a power IGBT," *IEEE Transactions on Nuclear Science*, vol. 44, pp. 2353–2357, Dec. 1997.

[10] Y. Apanovich, P. Blakey, R. Cottle, E. Lyumkis, B. Polsky, A. Shur, and A. Tcherniaev, "Numerical simulation of submicrometer devices including coupled nonlocal transport and nonisothermal effects," *IEEE Transactions on Electron Devices*, vol. 42, pp. 890–897, May 1995.

[11] M. N. Özişik, *Boundary Value Problems of Heat Conduction.* Dover Publications, Inc., 1968.

[12] S. M. Sze, *Physics of Semiconductor Devices.* John Wiley and Sons, 2 ed., 1981.

[13] C.-L. Tien, A. Majumdar, and F. M. Gerner, eds., *Microscale Energy Transport.* Taylor and Francis, 1998.

[14] W. V. Petegen, B. Geeraerts, W. Sansen, and B. Graindourze, "Electrothermal simulation and design of integrated circuits," *IEEE Journal of Solid-State Circuits*, vol. 29, pp. 143–146, Feb. 1994.